Supplementary Information for

Reversible structural change of $[Co_2Fe_2]$ complexes between diamagnetic hydrogen-bonded 1D chains and paramagnetic complexes within a layered structure of amphiphilic anions

Nozomi Mihara[a], Soyoka Iitsuka[a], Takuya Shiga[a], and Masayuki Nihei*[a]

[a] Department of Chemistry, Institute of Pure and Applied Sciences, University of Tsukuba, Tennodai1-1-1, Tsukuba, Ibaraki, 305-8571 (Japan).

Table of contents

S1 General methods S3

S2 Materials S4

S3 IR spectra of **1X**$_2$.....S5

S4 Magnetic susceptibility of **1X**$_2$ S6

S5 TG-DTA and DSC of **1X**$_2$ S7

S6 Single crystal X-ray structural analysis of **1X**$_2$.....S8

S7 PXRD of **1X**$_2$ S14

S8 Single crystal X-ray structural analysis of **1T**$_2$.....S15

S9 Magnetic susceptibility of **1T**$_2$.....S18

S10 IR spectra of **1T**$_2$ and **1X**$_2$ during heating and exposing to air.....S19

S11 TG-DTA of **1T**$_2$ S21

S12 References.....S22

S13 Explanation of an alert in CIFCHECK.....S23

S1 General methods

Infrared absorption spectra were measured on KBr pellet samples or by ATR method using a SHIMADZU IRAffinity-1 spectrometer. A UNISOKU CoolSpeK UV/CD (USP-203A) was used for temperature control in the variable temperature IR spectrum measurements. Samples for KBr method were prepared by press of samples between KBr crystals (3 mm × 3 mm) for IR measurement.

Magnetic susceptibility data were collected using a Quantum Design MPMS-5XL SQUID magnetometer. 10–20 mg of sample wrapped in aluminium foil was used as the measurement sample. Temperature dependence was measured with an applied magnetic field of 1 T with the scan rate of 1 K/min in the temperature range of 5–400 K. Magnetic data were corrected for the diamagnetism of the sample holder and the diamagnetism of the sample using Pascal's constants. The magnitude of $\chi_M T$ values of the holder for diamagnetic correction are 10^{-3} emu K at 5–400 K. The values of the diamagnetic corrections of the samples are -1.65×10^{-3} emu mol^{-1} and -1.37×10^{-3} emu mol^{-1} for $\mathbf{1X}_2$-A and $\mathbf{1T}_2$, respectively.

Thermogravimetric measurements were performed using Shimadzu DTG-60 and DSC-60Plus in the temperature range of 200 K to 450 K for DSC measurements and in the temperature range of room temperature to 400 K for TG-DTA measurements. The samples for DSC were prepared by placing 1–2 mg of sample in an aluminium pan, crimped and covered with a lid. The samples for TG-DTA were prepared by placing 5–15 mg of sample in an aluminium pan.

Powder X-ray diffraction (PXRD) measurements were performed on a powder X-ray diffractometer (BRUKER, D8 ADVANCE) with a CCD two-dimensional detector using the Mo-Kα line (λ = 1.5406 Å) as X-ray source. The measurements were performed in 2θ range of 3.5–35 º, every 0.01º, with an irradiation time of 1.5 s and tube voltage and current of 40 kV and 40 mA. The variable-temperature PXRD measurements were performed with TTK-450 (Anton Paar).

Elemental analysis was performed using a Perkin-Elmer Model 2400 organic elemental analyzer.

The detail of the X-ray structural analysis was described in Supplementary Section S6.

S2 Materials

$CoCl_2 \cdot 6H_2O$ (wako 030-03685), 4,4'-di-*tert*-butyl-2,2'-bipyridyl (Sigma-Aldrich 515477), methanol (Wako 137-01823), *tert*-butyl alcohol (Wako 025-03396) and *N*,*N*-dimethylformamide (Wako 045-02916) were purchased and used without further purification.

Preparation of $1X_2$-C for elemental analysis

1X$_2$-A was heated at 343 K and then cooled to room temperature. The resulting crystals were exposed to air to obtain **1X**$_2$-C as green crystals. Anal. calcd for $C_{170}H_{268}B_2Co_2Fe_2N_{28}O_{22}S_2$ (**1X**$_2 \cdot 6H_2O$): C, 60.31; H, 8.01; N, 11.64; found: C, 60.39; H, 7.96; N, 11.62; (0.08% error).

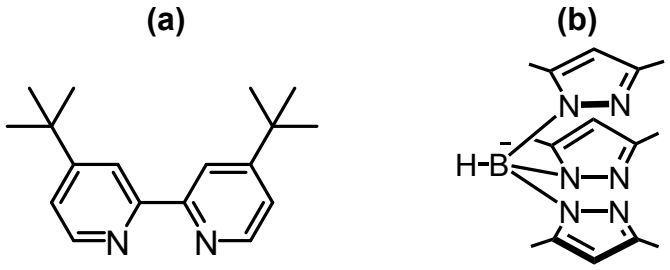

dtbbpy tp*

Figure S1 The schemes of (a) dtbbpy (4,4'-di-*tert*-butyl-2,2'-bipyridyl) and (b) tp* (hydrotris(3,5-dimethylpyrazol-1-yl)borate).

S3 IR spectra of $1X_2$

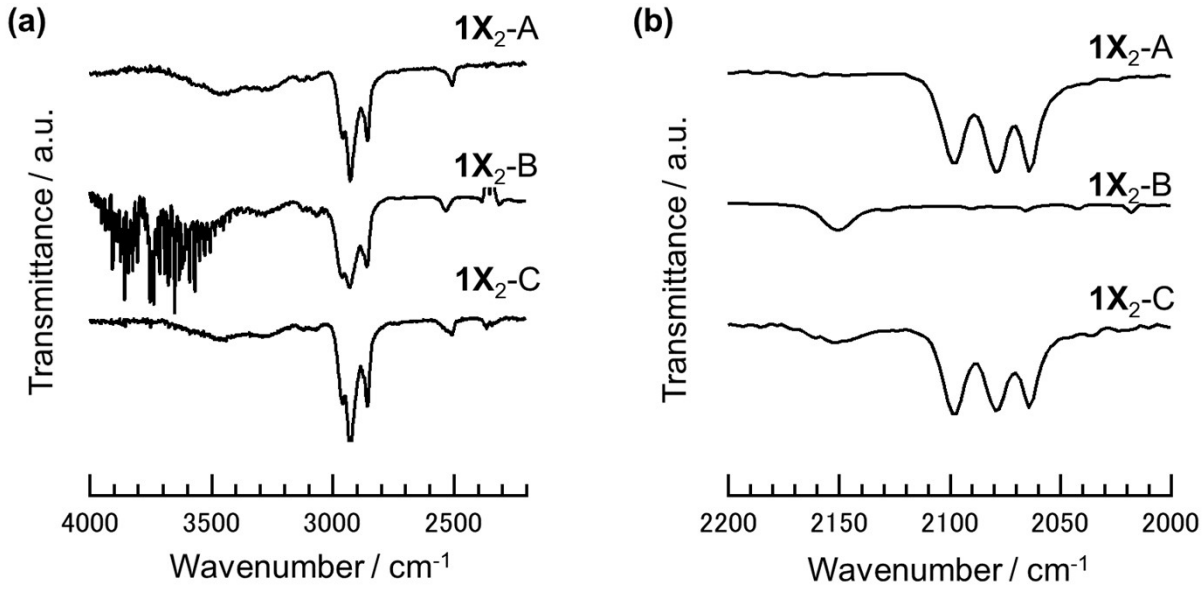

Figure S2 IR spectrum of **1X**$_2$-A–**1X**$_2$-C ((a) 4000–2200 cm^{-1}, (b) 2200–2000 cm^{-1}). The noisy spectrum (4000-3500 cm^{-1}) of 1**X**$_2$-B, formed by heating **1X**$_2$-A in IR machine, is presumably because of the temperature difference of the measurement of background (r.t.) and 1**X**$_2$-B (373 K).

Table S1 Stretching vibration values of bridging and terminal CN groups of **1**$(PF_6)_2 \cdot 2MeOH$[1] and **1X**$_2$.

	Bridging CN groups (cm^{-1})		Terminal CN groups (cm^{-1})	
	Fe^{III}-CN-Co^{II}	Fe^{II}-CN-Co^{III}	Fe^{III}-CN	Fe^{II}-CN
1$(PF_6)_2 \cdot 2MeOH$ (335 K) / (HS)	2152	-	2127	-
1$(PF_6)_2 \cdot 2MeOH$ (220 K) / (LS)	-	2098, 2077	-	2070
1X$_2$-A	-	2097, 2079	-	2064
1X$_2$-B	2150	-	2129	-
1X$_2$-C	2149	2097, 2077	-	2064

S4 Magnetic susceptibility of $\mathbf{1X_2}$

The first and the fourth heating/cooling cycles of magnetic susceptibility measurements of $\mathbf{1X_2}$-A are shown in Figure S3(a) and (b), respectively. The heating process of Figure S3(a) is same as the data in Figure 4(c). The $\chi_M T$ value is 0.31 emu mol^{-1} K at 5 K, which is slightly larger than the expected value ($\chi_M T$ = 0 emu mol^{-1} K) for the LS state of $\mathbf{1}^{2+}$ consisting of two *ls*-Fe^{II} ions (S = 0) and two *ls*-Co^{III} ions (S = 0), suggesting that the complex is in the LS state but contains a small amount of paramagnetic impurities. The $\chi_M T$ value increases rapidly when the temperature increases from 300 K to 320 K. This rapid increase in $\chi_M T$ value is attributed to the thermally induced ETCST from the LS to the HS state. The $\chi_M T$ value was 6.15 emu mol^{-1} K at 400 K. The expected value for the HS state of $\mathbf{1}^{2+}$ consisting of two *ls*-Fe^{III} ions (S = 1/2, g = 2.7) and two *hs*-Co^{II} ions (S = 3/2, g = 2.3) without magnetic interaction[2] is $\chi_M T$ = 6.33 emu mol^{-1} K, which indicates that all of $\mathbf{1}^{2+}$ is in HS state at 400 K. Therefore, the complex was in the LS state at room temperature and completely changed to the HS state.

During the cooling process from 240 K to 100 K, the $\chi_M T$ value shows a gradual decrease to 4.77 emu mol^{-1} K at 100 K, suggesting that about 25% of $\mathbf{1}^{2+}$ changed to the LS state. When the cycle of heating and cooling in the range of 5–400 K was repeated four times, the plot resulted in a gradual transition in the range of 130–240 K.

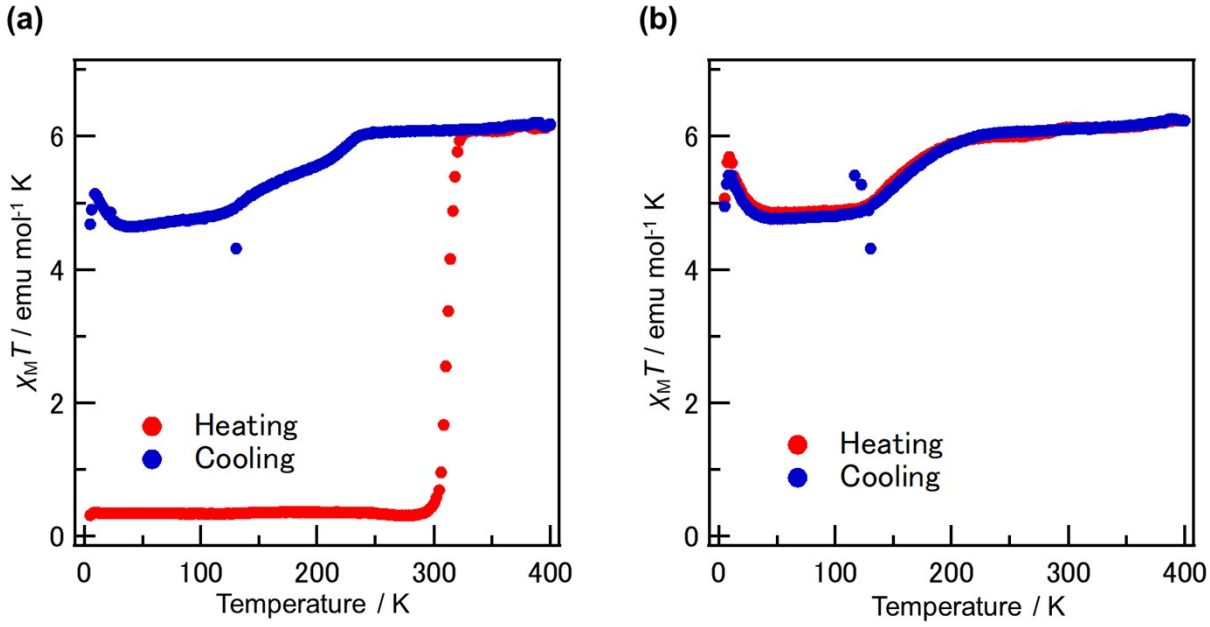

Figure S3 $\chi_M T$–T plot of $\mathbf{1X_2}$-A of (a) The first cycle and (b) The fourth cycle.

S5 TG-DTA and DSC of $1X_2$

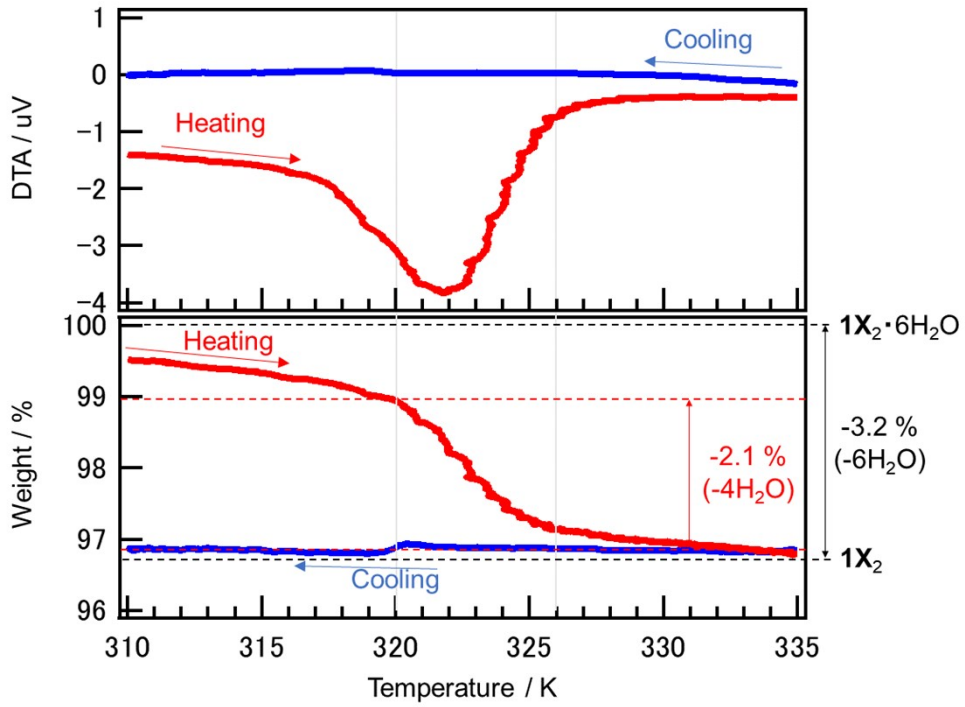

Figure S4 TG-DTA of $\mathbf{1X_2}$-A (Scan rate : 1 K min^{-1}).

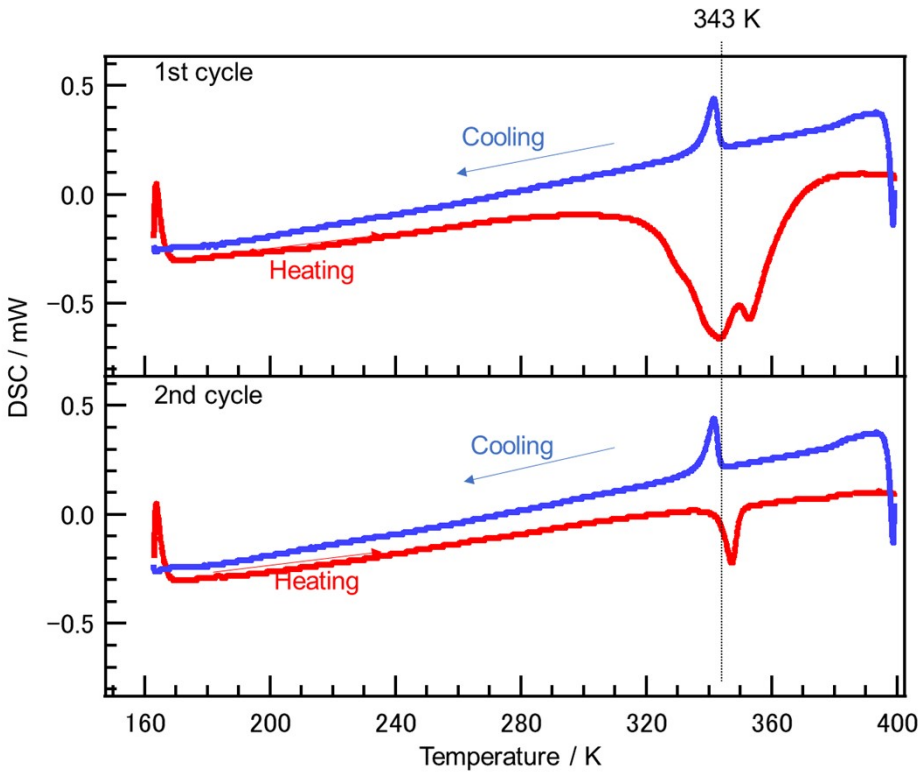

Figure S5 DSC of $\mathbf{1X_2}$-A (Scan rate : 10 K min^{-1}).

S6 Single crystal X-ray structural analysis of $1X_2$

Single crystals were mounted with Paratone-N on MicroLoops or glue on glass capillary. Diffraction data were collected using a Bruker SMART APEX II ULTRA diffractometer equipped with a CCD type area detector. The data was collected with graphite-monochromated Mo-Kα radiation (λ = 0.71073 Å). The data frames were integrated using the SAINT program and merged to give a unique data set for structure determination. An absorption correction was performed using SADABS. The structure was solved by direct methods and refined on F^2 by the full-matrix least-squares methods using SHELXTL package (Bruker Analytical X-ray systems). Non-hydrogen atoms were refined with anisotropic thermal parameters. Hydrogen atoms were included in calculated positions and refined with isotropic thermal parameters riding on those of the parent atoms. CCDC 2333265–2333267 contain the supplementary crystallographic data for this paper. These data can be obtained free of charge via www.ccdc.cam.ac.uk/conser/trieving.html (or from the Cambridge Crystallographic Data Centre, 12, Union Road, Cambridge CB21EZ, UK; fax: (+44)1223-336-033; or deposit@ccdc.cam.ac.uk). Crystallographic parameters are summarized in Table S5 and S8.

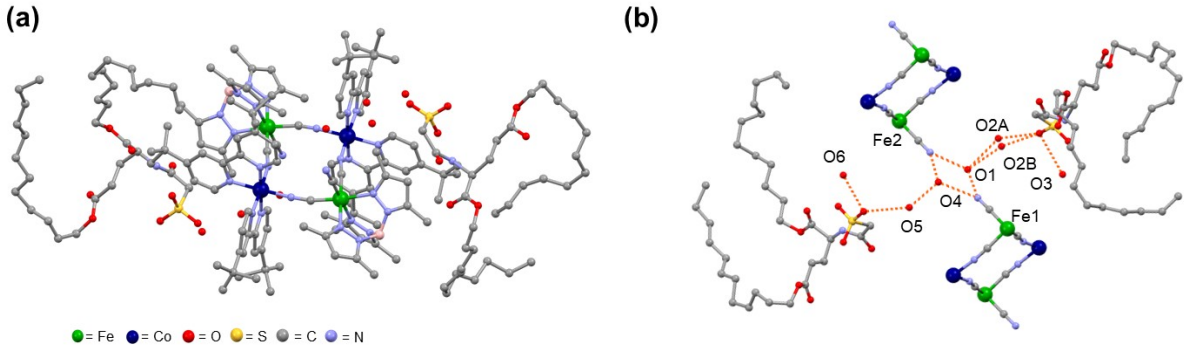

Figure S6 (a) Single crystal X-ray structure of $\mathbf{1X_2}$-A at 200 K. Hydrogen atoms are omitted for clarity. (b) The hydrogen-bonding network of $\mathbf{1X_2}$-A and water molecules. Hydrogen atoms and ligands are omitted for clarity.

Table S2 The distances (Å) of the coordination bonds of $\mathbf{1X_2} \cdot 6H_2O$ ($\mathbf{1X_2}$-A) obtained by X-ray structural analysis.

Co(1)-N(dtbbpy)	1.942(10) 1.921(10) 1.933(11) 1.931(9)	Co(2)-N(dtbbpy)	1.935(10) 1.941(10) 1.939(10) 1.903(10)
Co(1)-N(NC)	1.885(10) 1.931(13)	Co(2)-N(NC)	1.919(10) 1.884(10)
Co(1)-N(ave)	1.924(11)	**Co(2)-N(ave)**	1.920(10)
Fe(1)-N(tp*)	2.046(11) 2.042(10) 2.040(10)	Fe(2)-N(tp*)	2.083(10) 2.044(11) 2.016(11)
Fe(1)-C(CN)	1.874(12) 1.854(14) 1.857(14)	Fe(2)-C(CN)	1.916(13) 1.868(13) 1.919(12)
Fe(1)-N(ave)	2.043	**Fe(2)-N(ave)**	2.048(11)
Fe(1)-C(ave)	1.862(13)	**Fe(2)-C(ave)**	1.901(13)

Table S3 The distances (Å) of the hydrogen-bonds of $\mathbf{1X_2} \cdot 6H_2O$ ($\mathbf{1X_2}$-A) obtained by X-ray structural analysis.

O(1)-N(NC)	2.809 3.019	O(4)-N(NC)	3.030 2.749
O(1)-O(2A)	2.857	O(4)-O(5)	2.579
O(1)-O(2B)	2.888	O(5)-O(SO_3)	3.015
O(2A)-O(SO_3)	2.892	O(6)-O(SO_3)	2.985
O(2B)-O(SO_3)	2.640	O(3)-O(SO_3)	3.393

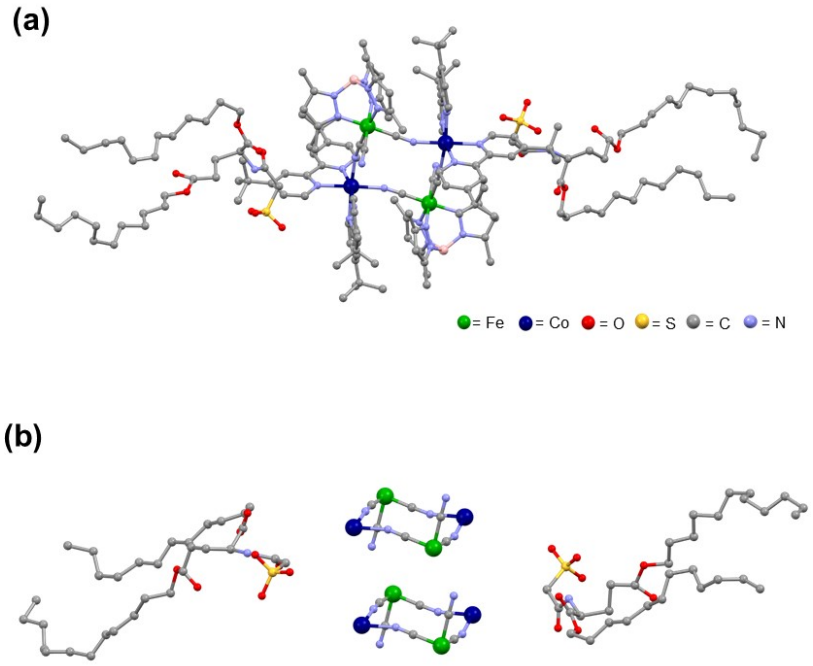

Figure S7 (a) Single crystal X-ray structure of $\mathbf{1X_2}$-B at 200 K. Hydrogen atoms are omitted for clarity. (b) The arrangement of $\mathbf{1}^{2+}$ and $\mathbf{X}^{-}$ in $\mathbf{1X_2}$-B. Hydrogen atoms and ligands are omitted for clarity.

Table S4 The distances (Å) of the coordination bonds of $\mathbf{1X_2}$ ($\mathbf{1X_2}$-B) obtained by X-ray structural analysis.

Co(1)-N(dtbbpy)	2.11(2) 2.12(3) 2.10(3) 2.18(3)	Co(2)-N(dtbbpy)	2.171(15) 2.132(17) 2.11(3) 2.09(3)
Co(1)-N(NC)	2.08(3) 2.14(4)	Co(2)-N(NC)	2.07(3) 2.09(3)
Co(1)-N(ave)	2.12(4)	**Co(2)-N(ave)**	2.11(3)
Fe(1)-N(tp*)	1.98(3) 2.01(2) 2.00(2)	Fe(2)-N(tp*)	1.99(3) 2.05(2) 1.94(2)
Fe(1)-C(CN)	1.87(3) 1.91(4) 1.90(3)	Fe(2)-C(CN)	1.80(5) 1.97(3) 1.96(4)
Fe(1)-N(ave)	1.97(3)	**Fe(2)-N(ave)**	1.99(3)
Fe(1)-C(ave)	1.89(4)	**Fe(2)-C(ave)**	1.91(4)

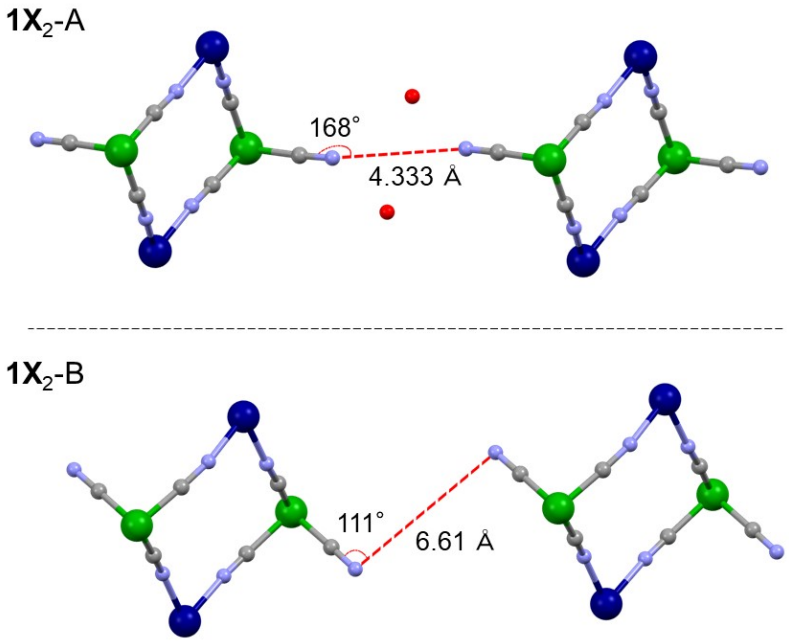

Figure S8 The comparison of the distances between terminal CN groups of neighbouring $\mathbf{1}^{2+}$ molecules in the crystal structure of $\mathbf{1X_2}$-A and $\mathbf{1X_2}$-B.

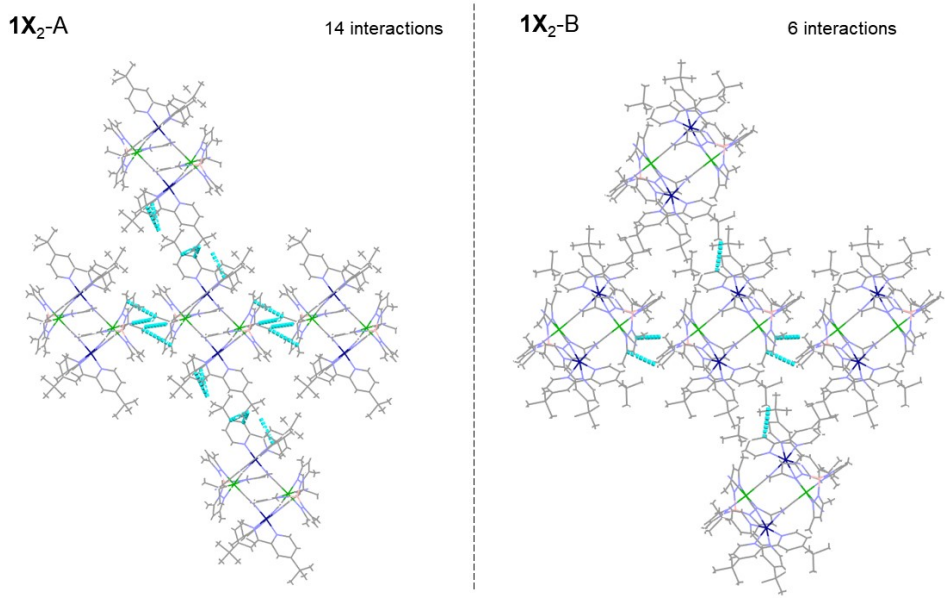

Figure S9 The comparison of the numbers of CH-π interactions (light blue lines) between a molecule of $\mathbf{1}^{2+}$ and neighbouring four molecules of $\mathbf{1}^{2+}$ in $\mathbf{1X_2}$-A and $\mathbf{1X_2}$-B.

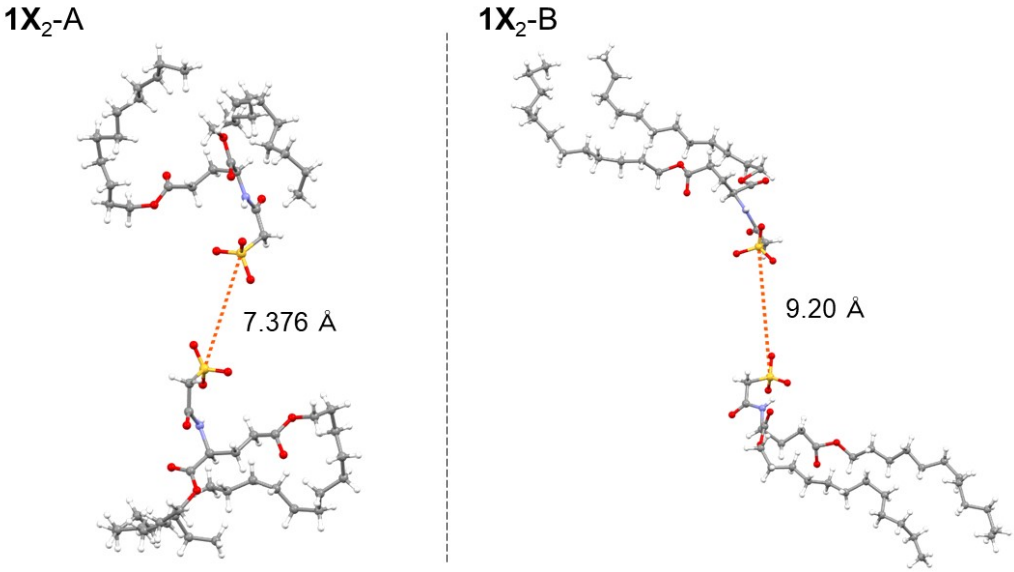

Figure S10 The comparison of the distances between S atoms and the structure of alkyl chains of $\mathbf{X}^-$ of in **1X**$_2$-A and **1X**$_2$-B.

Table S5 Crystallographic parameters and mesurement conditions of $\mathbf{1X_2} \cdot 6H_2O$ ($\mathbf{1X_2}$-A) and $\mathbf{1X_2}$ ($\mathbf{1X_2}$-B).

	$\mathbf{1X_2}$-A	$\mathbf{1X_2}$-B
Empirical formula	$C_{170}H_{256}B_2Co_2Fe_2N_{28}O_{22}S_2$	$C_{170}H_{250}B_2Co_2Fe_2N_{28}O_{16}S_2$
Formula weight	3359.31	3257.27
Temperature / K	200(2)	200(2)
Wavelength / Å	0.71073	0.71073
Crystal system	Triclinic	Triclinic
Space group	$P\bar{1}$	$P\bar{1}$
a / Å	12.8879(8)	13.052(12)
b / Å	17.7778(12)	16.203(15)
c / Å	22.5479(15)	23.83(2)
α / °	75.892(1)	77.546(9)
β / °	79.585(1)	78.183(8)
γ / °	71.793(1)	72.120(8)
V / Å^3	4728.7(5)	4631(2)
Z	1	1
Density (calculated) / Mg m^{-3}	1.180	1.170
Absorption coefficient / mm^{-1}	0.411	0.416
F (000)	1796	1742
Theta range for data collection	1.390 to 27.500	0.885 to 27.491
Reflections collected	56005	47656
Independent reflections	41960	39142
R(int)	0.0256	0.1189
Completeness / %	99.8	99.4
Data / restraints / parameters	41960 / 1262 / 2064	39142 / 2575 /1946
Goodness-of-fit on F^2	1.013	1.117
Final R indices [I>2sigma(I)]	$R1$ = 0.0773, $wR2$ = 0.2057	$R1$ = 0.1631, $wR2$ = 0.3473
R indices (all data)	$R1$ = 0.1249, $wR2$ = 0.2508	$R1$ = 0.3697, $wR2$ = 0.5171
Absolute structure parameter	0.31(3)	0.25(8)
Largest diff. peak and hole / e. Å^{-3}	0.851 and -0.720	1.493 and -1.175

S7 PXRD of $1X_2$

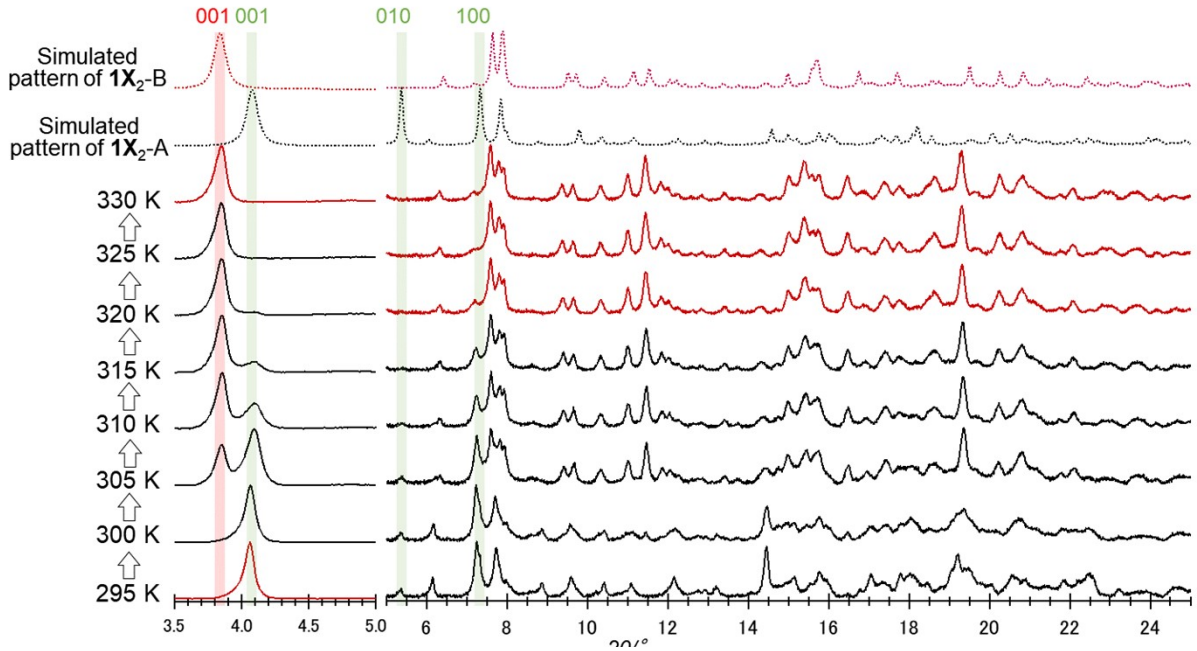

Figure S11 The change of PXRD patterns when $\mathbf{1X_2}$-A is heated from 295 to 330 K. The calculated patterns of $\mathbf{1X_2}$-A and $\mathbf{1X_2}$-B from data of the single crystal structural analysis are also shown.

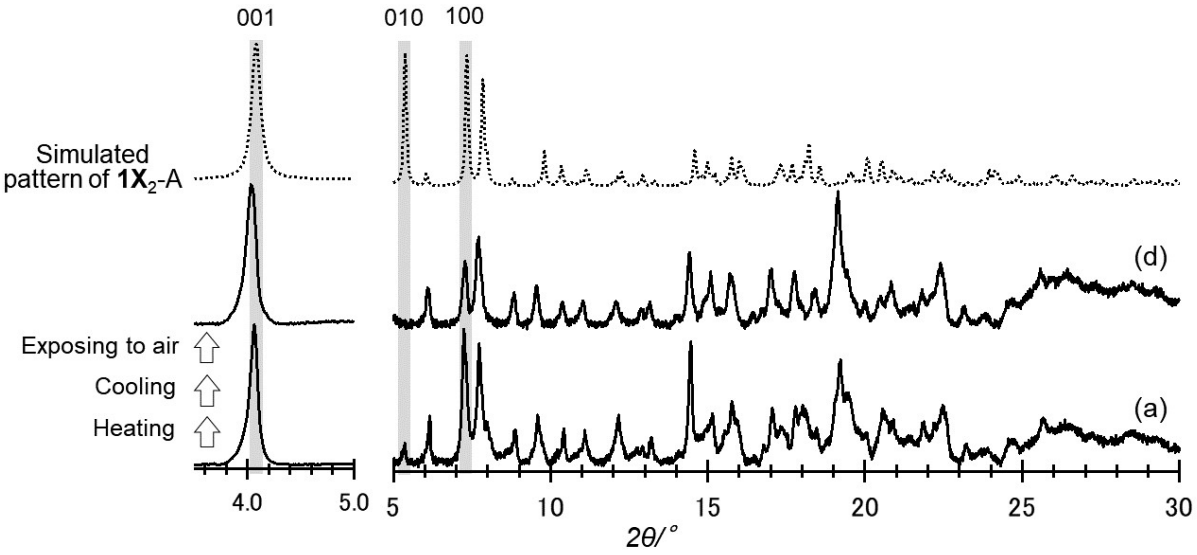

Figure S12 The change of PXRD patterns when $\mathbf{1X_2}$-A is heated, cooled, and exposed to air. The patterns of (a) $\mathbf{1X_2}$-A and (d) $\mathbf{1X_2}$-C are identical to (a) and (d) in Figure 5. The calculated patterns of $\mathbf{1X_2}$-A from single crystal data are also shown. The comparison of the patterns suggests that the structures of $\mathbf{1X_2}$-A and $\mathbf{1X_2}$-C are similar and $\mathbf{1X_2}$-C would have a layered structure and 1D chain LS state as $\mathbf{1X_2}$-A.

S8 Single crystal X-ray structural analysis of $1T_2$

The detail of single crystal X-ray structural analysis was described in Supplementary Section S6.

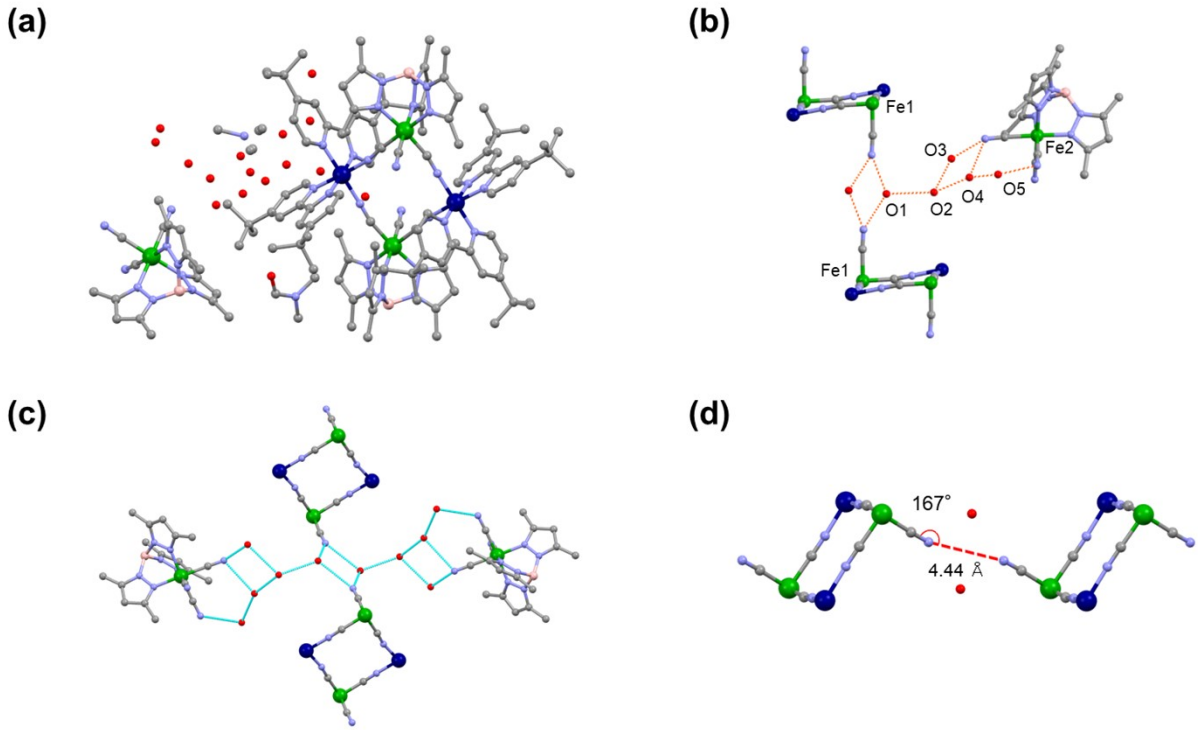

Figure S13 (a) Single crystal X-ray structure of $\mathbf{1T_2} \cdot 18H_2O \cdot 4DMF$ at 120 K. Hydrogen atoms are omitted for clarity. (b) The hydrogen-bonds of neighbouring $\mathbf{1}^{2+}$ molecules, $\mathbf{T}^{-}$, and water molecules in the crystal structure of $\mathbf{1T_2} \cdot 18H_2O \cdot 4DMF$. (c) The 1D chain hydrogen-bonding network of $\mathbf{1T_2}$ with water molecules. (d) The distance between terminal CN groups of neighbouring $\mathbf{1}^{2+}$ molecules in the crystal structure of $\mathbf{1T_2} \cdot 18H_2O \cdot 4DMF$.

Table S6 The distances (Å) of the coordination bonds of $\mathbf{1T_2} \cdot 18H_2O \cdot 4DMF$ obtained by X-ray structural analysis.

Fe(1)-N(tp*)	2.052(2) 2.042(2) 2.049(2)	Co(1)-N(dtbbpy)	1.932(2) 1.933(2) 1.926(2) 1.924(2)
Fe(1)-C(CN)	1.883(3) 1.894(3) 1.895(3)	Co(1)-(NC)	1.898(2) 1.904(2)
Fe(1)-N(ave) **Fe(1)-C(ave)**	2.048(2) 1.891(3)	**Co(1)-N(ave)**	1.919(2)

Table S7 The distances (Å) of the hydrogen-bonds of $\mathbf{1T_2} \cdot 18H_2O \cdot 4DMF$ obtained by X-ray structural analysis.

O(1)-N(NC)	3.01 2.80	O(1)-O(2) O(2)-O(3)	2.82 2.93
O(2)-O(4)	2.84	O(3)-N(NC)	2.93
O(4)-N(NC)	3.05	O(4)-O(5)	2.90
O(5)-N(NC)	2.98		

Table S8 Crystallographic parameters and mesurement conditions of $\mathbf{1T}_2 \cdot 18H_2O \cdot 4DMF$.

	$\mathbf{1T}_2$
Empirical formula	$C_{156}H_{248}B_4Co_2Fe_4N_{48}O_{22}$
Formula weight	3532.51
Temperature / K	120
Wavelength / Å	0.71073
Crystal system	Triclinic
Space group	$P\bar{1}$
a / Å	12.484(3)
b / Å	16.445(4)
c / Å	22.402(5)
α / °	95.341(4)
β / °	92.874(3)
γ / °	94.153(4)
V / Å^3	4559.6(17)
Z	1
Density (calculated) / Mg m^{-3}	1.286
Absorption coefficient / mm^{-1}	0.562
F (000)	1874
Theta range for data collection	1.473 to 27.499
Reflections collected	27629
Independent reflections	20042
R(int)	0.0328
Completeness / %	97.7
Data / restraints / parameters	20042 / 183 / 1267
Goodness-of-fit on F^2	1.008
Final *R* indices [*I*>2sigma(*I*)]	*R*1 = 0.0537, *wR*2 = 0.1189
R indices (all data)	*R*1 = 0.0874, *wR*2 = 0.1361
Largest diff. peak and hole / e. Å^{-3}	0.978 and -0.826

S9 Magnetic susceptibility of $\mathbf{1T_2}$

The first and the second heating/cooling cycles of magnetic susceptibility measurement of $\mathbf{1T_2}$ are shown in Figure S14(a) and (b), respectively. The $\chi_M T$ value was 1.07 emu mol^{-1} K at 5 K, which is close to the expected value for the LS state of $\mathbf{1}^{2+}$ and two *ls*-Fe^{III} ions ($S = 1/2$, $g = 2.7$) of two $\mathbf{T}^-$ anions (expected value: $\chi_M T = 1.37$ emu mol^{-1} K). The $\chi_M T$ value increases rapidly when the temperature increases from 296 K to 310 K. This rapid increase in $\chi_M T$ value is attributed to the thermally induced ETCST of $\mathbf{1}^{2+}$ from the LS to the HS state. The $\chi_M T$ value is 6.27 emu mol^{-1} K at 400 K. This value is smaller than the expected value ($\chi_m T = 7.69$ emu mol^{-1} K) for the HS state of $\mathbf{1}^{2+}$ (expected value: $\chi_M T = 6.33$ emu mol^{-1} K) consisting of two *ls*-Fe^{III} ions ($S = 1/2$, g = 2.7) and two *hs*-Co^{II} ions ($S = 3/2$, g = 2.3) without magnetic interaction[2], and two *ls*-Fe^{III} ions ($S = 1/2$, $g = 2.7$) in two molecules of $\mathbf{T}^-$ (expected value: $\chi_M T = 1.37$ emu mol^{-1} K), suggesting that most of $\mathbf{1}^{2+}$ changed to the LS state.

During the cooling process from 270 K to 150 K, the $\chi_M T$ value shows a gradual decrease to reach to 3.55 emu mol^{-1} K at 100 K, suggesting that about 40% of $\mathbf{1}^{2+}$ changed to the LS state. When the cycle of heating and cooling in the range of 5–400 K is repeated again, the plot shows a gradual transition in the range of 150–270 K (Figure S14(b)). The $\chi_M T$ value is 6.74 emu mol^{-1} K at 400 K, suggesting that most of $\mathbf{1}^{2+}$ is in the HS state.

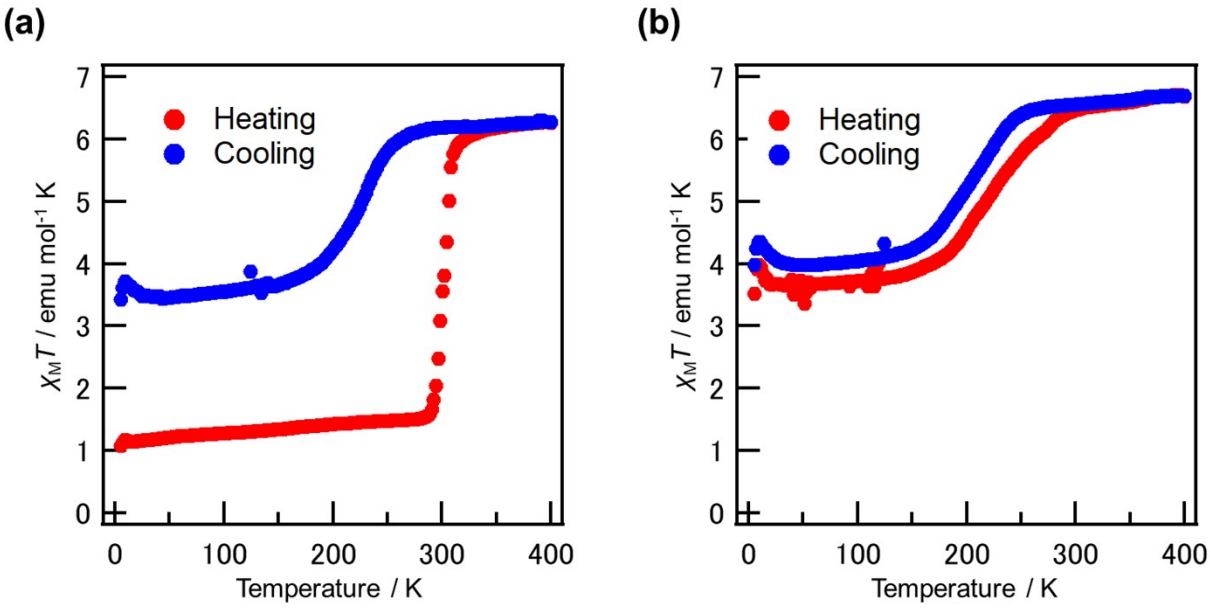

Figure S14 $\chi_M T$–T plot of $\mathbf{1T_2} \cdot 18H_2O \cdot 4DMF$ of (a) The first cycle and (b) The second cycle.

S10 IR spectra of $1T_2$ and $1X_2$ during heating and exposing to air

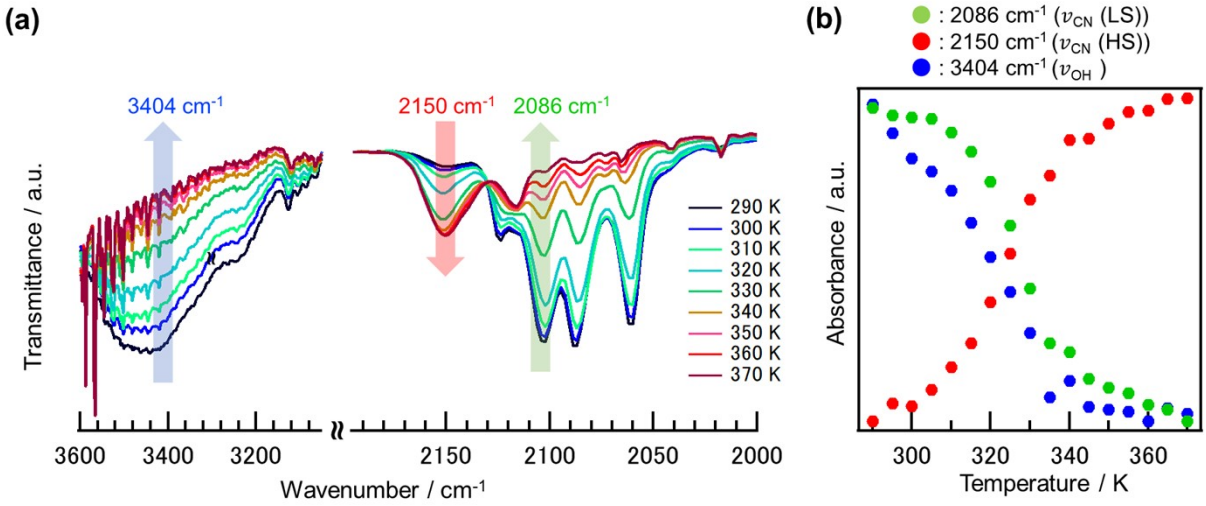

Figure S15 (a) IR spectra measured by KBr method when $1T_2 \cdot 18H_2O \cdot 4DMF$ was heated from 290 to 370 K. (b) The temperature dependence of absorbances at 2086 cm^{-1} (ν_{CN} (LS), blue circles), 2150 cm^{-1} (ν_{CN} (HS), red circles), and 3404 cm^{-1} (ν_{OH}, green circles).

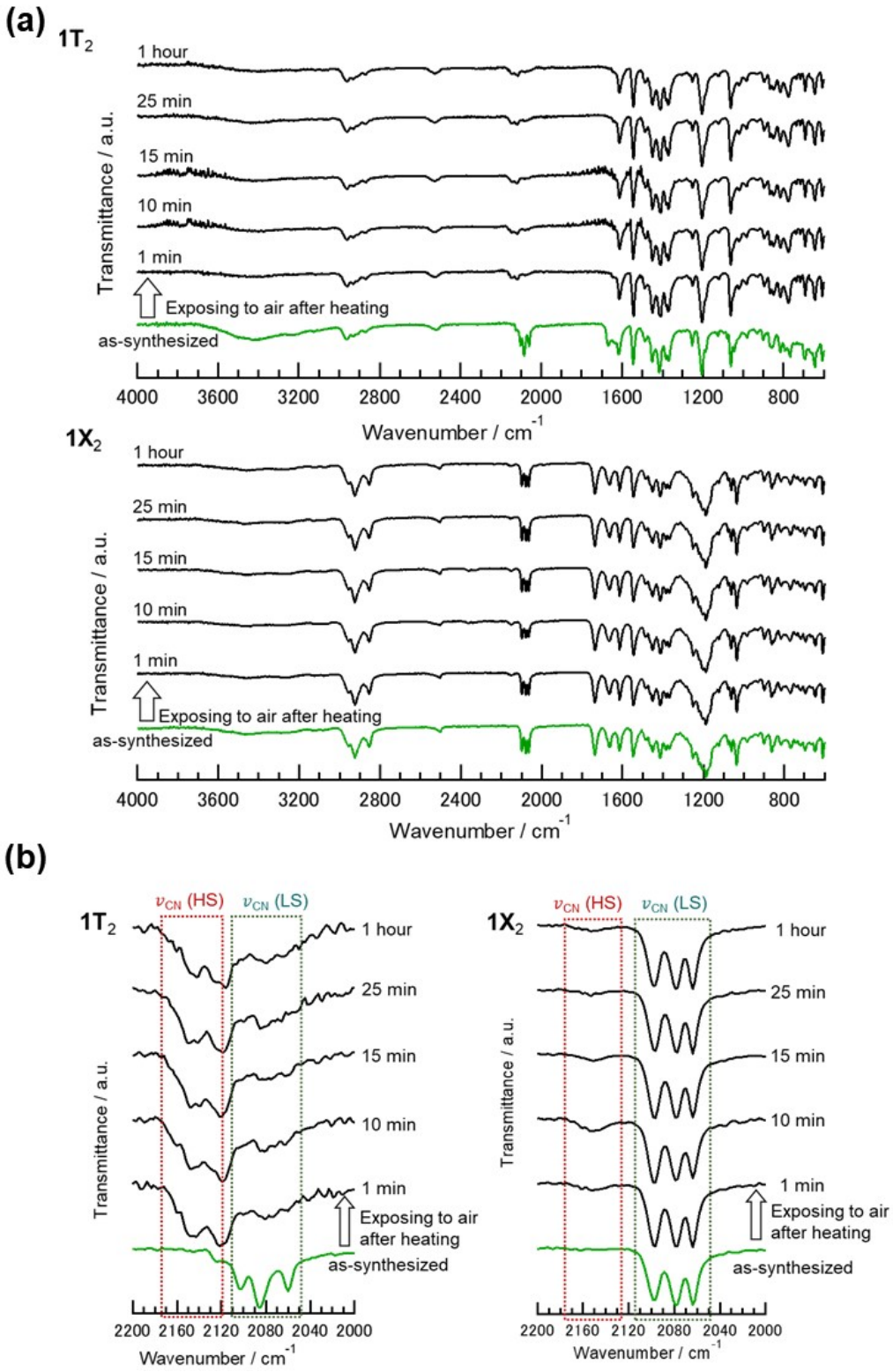

Figure S16 IR spectra of $\mathbf{1T}_2$ and $\mathbf{1X}_2$ when they were heated and then exposed to air for 1 hr. (a) 600–4000 cm^{-1} and (b) 2000–2200 cm^{-1}.

S11 TG-DTA of $1T_2$

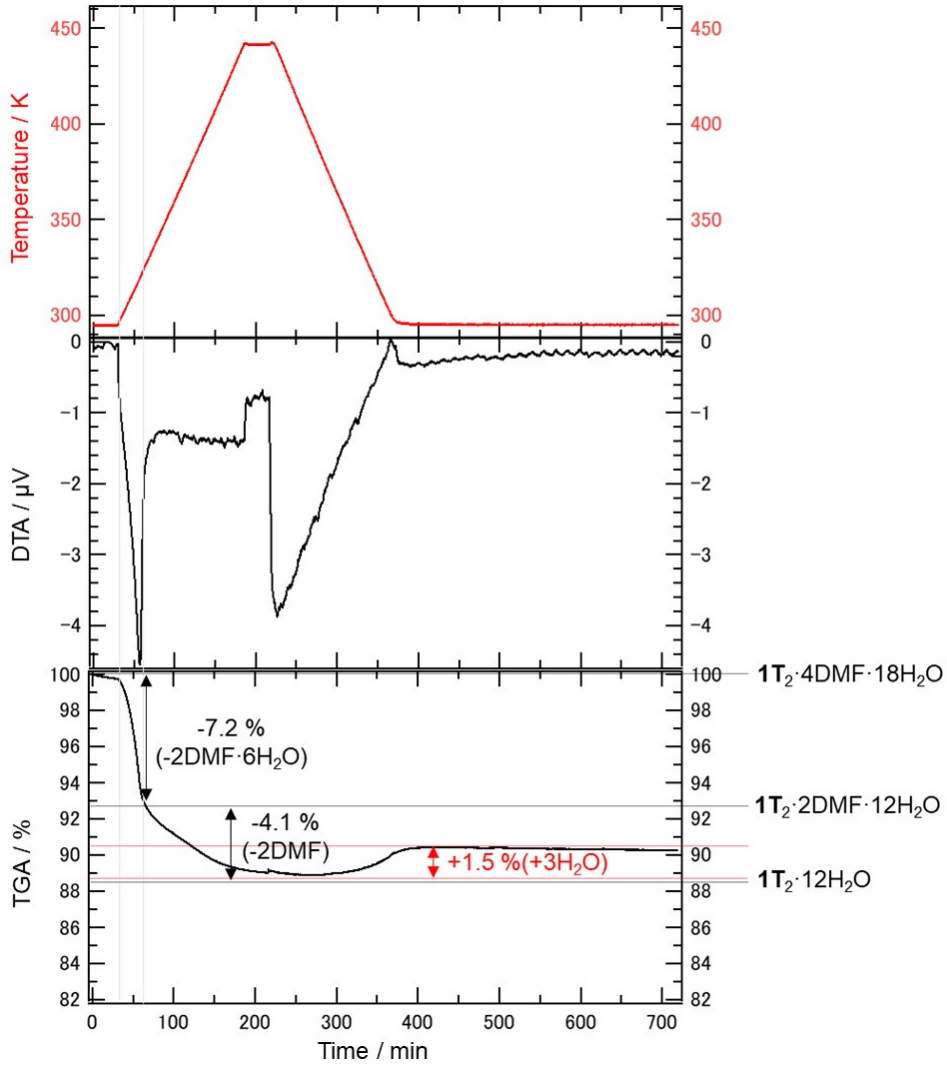

Figure S17 TG-DTA of $\mathbf{1T_2}$.

S12 References

[1] M. Nihei, Y. Sekine, N. Suganami, K. Nakazawa, A. Nakao, H. Nakao, Y. Murakami, H. Oshio, *J. Am. Chem. Soc.* **2011**, *133*, 3592-3600.

[2] a) D. Li, R. Clérac, O. Roubeau, E. Harté, C. Mathonière, R. L. Bris, S. M. Holmes, *J. Am. Chem. Soc.* **2008**, *130*, 252-258; b) M. Nihei, Y. Sekine, N. Suganami, H. Oshio, *Chem. Lett.* **2010**, *39*, 978-979.

S13 Explanation of an alert in CIFCHECK

Datablock: 1X2-B

PLAT084_ALERT_3_A High wR2 Value (i.e. > 0.25) ..... 0.52 Report

The crystal of **1X**$_2$-B was obtained by drying a single crystal of **1X**$_2$-A mounted on a goniometer of an X-ray diffractometer with N_2 gas flow. The temperature of the N_2 gas has been kept at 260 K for a day and then was increased gradually to 310 K. The crystallinity of the crystal decreased during the transformation, resulting in high wR2 value. In addition, the disorder of $\mathbf{X}^-$ having two C12 alkyl chains also can cause high wR2 value.